Journal of Molecular Liquids 389 (2023) 122861

Contents lists available at ScienceDirect

Journal of Molecular Liquids

journal homepage: www.elsevier.com/locate/molliq

New approach to instantaneous polarizable electrostatic embedding of the solvent

M.B. Kiataki, M.T. do N. Varella *, K. Coutinho *

Instituto de Física, Universidade de São Paulo, Rua do Matão 1371 CP 66318, CEP 05508-090 São Paulo, SP, Brazil

A B S T R A C T

The sequential quantum mechanics/molecular mechanics (S-QM/MM) method efficiently computes solvent effects on the electronic properties of solutes. The protocol involves two steps: solute-solvent configurations are generated from MM simulations, while the solute properties are computed in the subsequent QM step. A well-known difficulty within the S-QM/MM framework is the description of the polarization of the MM partition (electrostatic embedding) in case the electronic structure of the solute undergoes sudden changes, such as in electronic excitation, electron attachment or detachment processes. To improve the description of the electronic polarization of the solvent, we propose the self-consistent S-QM/MM polarizable electrostatic embedding (scPEE-S-QM/MM) method, which generates individual atomic charges for the solvent molecules due to solute-solvent and solvent-solvent polarization. The electronic properties calculated for the neutral and anion states of 1-methyl-4-nitroimidazole were found to be significantly affected by solvent polarized electrostatic embeddings obtained for different solute electronic states. Finally, the method also provides accurate results for bulk water.

1. Introduction

Complex molecular systems pose a formidable challenge to computational models. Although quantum mechanical (QM) methods can accurately describe the electronic structure of molecules, their use is still limited by the numerical cost associated with the size and complexity of the systems of interest. Several phenomena, such as bond formation and breaking, charge transfer, electronic excitation and electron attachment, take place in relatively localized regions, where QM methods can be applied, while the surroundings can be treated with the less expensive molecular mechanical (MM) techniques. This hybrid quantum mechanical/molecular mechanical (QM/MM) approach emerged in 1976 to study enzymatic reactions [1] and since then has been applied in several studies of chemical and biochemical systems [2–6]. The relevance and impact of the QM/MM approach were recognized in 2013 with the Nobel Prize in Chemistry [4].

Several flavors of QM/MM methods have been developed [2,4,7–10]. They essentially differ in the way the QM and MM regions are defined and coupled, the scheme used to compute the QM/MM energies, and whether the QM and MM calculations are performed simultaneously [2] or sequentially [11–13]. The accuracy of QM/MM methods depends not only on the choice of methods to describe the QM and MM components individually, but also on the model that accounts for the interaction between the quantum and classical regions. The coupling may involve electrostatic, polarization and dispersion intermolecular interactions, as well as bonded interactions between QM and MM atoms. The mutual polarization of the quantum and classical partitions is ignored in the simplest mechanical embedding scheme, which describes the QM-MM electrostatic interaction at the MM level with effective atomic charges. This shortcoming is partly overcome in the electrostatic embedding (EE-QM/MM) approach. The potential generated by the effective charges of the MM atoms is incorporated into the QM Hamiltonian, thus allowing for the EE-induced polarization of the QM subsystem. Despite the neglect of the polarization of the MM subsystem, the EE-QM/MM approach has been widely employed [2,9,14].

The EE-QM/MM approach can be improved by extending the QM region into the MM one, i.e., by incorporating some of the MM particles into the QM partition [15–17]. Since the QM subsystem and part of the original MM subsystem are now treated on the same footing (quantum mechanically), mutual polarization is accounted for within the extended QM region, although the numerical effort scales rapidly with the number of quantum particles. Alternatively, the EE-QM/MM approach can incorporate the solvent polarization with classical polarizable force fields, which increase the numerical effort associated with the calculation of forces and energies in the MM subsystem. The induced dipole model [18,19], the fluctuating charge model [20,21], and the Drude oscillator model [22,23] are representative examples of polarizable MM schemes. While the polarized EE-QM/MM can be viewed

* Corresponding authors.
E-mail addresses: kiatakimatheus@gmail.com, kiataki@usp.br (M.B. Kiataki), mvarella@if.usp.br (M.T. do N. Varella), kaline@if.usp.br (K. Coutinho).

https://doi.org/10.1016/j.molliq.2023.122861
Received 28 February 2023; Received in revised form 8 August 2023; Accepted 16 August 2023
Available online 23 August 2023

as improved with respect to EE-QM/MM, its use is still not widespread probably due to the additional computational cost and the limited availability of polarizable force fields in standard software packages.

The polarization of the electrostatic embedding generally affects absorption spectra, excitation, ionization and attachment energies, the interaction energy in water clusters, as well as the dipole moment of liquid water [5,10,24,25]. Polarization effects are also particularly relevant for charged quantum system embedded in solvents or complex biological media. In the present study, we propose a method, named self-consistent sequential QM/MM polarizable electrostatic embedding (scPEE-S-QM/MM), to polarize the electrostatic embedding, therefore accounting for mutual polarization in the sequential QM/MM (S-QM/MM) framework [11,12]. Unlike the traditional on-the-fly QM/MM method, which performs QM calculations for each MM simulation step (typically around a few hundred thousand QM calculations), in the sequential approach the MM simulation is firstly carried out to generate the solute-solvent configurations. The averaged properties of the solvated solute are then obtained from QM calculations carried out for a set of statistically uncorrelated configurations (typically hundreds of QM calculations). Therefore, the sequential approaches have the advantage of lower computational cost, although with the disadvantage of uncoupling the MM simulation with the QM calculation (not allowing the study of chemical reactions and other processes where the electronic effects are important during the nuclear dynamics). The S-QM/MM method has been successfully used to study electronic properties of solute in solutions [12,13,26] and the inclusion of the solute polarization caused by the solvent in the MM and QM stages brought an important contribution to the understanding of solvent effects, mainly in molecules where the electronic structure is very soft and polarizable, such as molecular probes or push-pull molecules [27–30]. In the MM stage, the atomic charges of the solute in the classical force field were replaced by polarized atomic charges obtained by a self-consistent iterative procedure [27,30] or by continuum models [28,31]. In the QM stage, the solute is usually embedded in the electrostatic field of solvent molecules described with the atomic charges of classical force fields (traditional EE approach). Thus, the solute wave function is polarized by the surrounding static environment which is not back polarized. Although the EE approach takes into account the average solvent polarization implicitly included in the atomic charges of the force fields, improved recent approaches have considered more realistically the polarized solvent electrostatic embedding. For instance, in the Self-Consistent Electrostatic Embedding (SCEE) method [24,32] the atomic charges of the solvent molecules are obtained from a few QM calculations for a homogeneous solution, although the same set of atomic charges are used for all solvent molecules even in solute-solvent systems. The average solvent polarization, described by the atomic charges employed for all the molecules comprising the EE, improves considerably the description of the liquid phase, e.g., the molecular dipole and higher multipole moments in solution [24,32]. However, it might not suitably describe the response to sudden changes in the electronic structure of the solute caused by electronic excitation or electron attachment/detachment. In these cases, the electron density of the solvent molecules is quickly polarized, much faster than the relaxation of the solvent atoms around the solute, and the individual response of the solvent molecules should be important. This shortcoming is overcome in the present scPEE-S-QM/MM scheme, where both solute-solvent and solvent-solvent fast mutual polarization are considered by recalculating the atomic charges of each individual molecule surrounded by the electrostatic embedding of all remaining molecules through QM calculations, with the solute in the modified electronic state. We discuss applications to negative ion states of a radiosensitizer molecule in aqueous solution and also to pure liquid water. Transient anion states formed by the attachment of secondary electrons to (bio)molecules, are known to play a role in radiobiology, in particular DNA damage induced by dissociative electron attachment reactions [33–37]. These detrimental reactions can be beneficial in chemo-radiation treatments if directed to the tumor cells. The nitroimidazoles are exemplar electron-affinic radiosensitizing drugs [38,39], which can enhance the efficiency of radiation treatments. Several recent studied have tried to connect the formation of transient anion states with the bioactivity of nitroimidazoles [40–46], also paying attention to solvent-induced effects [47,48].

Here, we consider three anion states of the 1-methyl-4-nitroimidazole (1M4NI), referred to as π_1^*, π_2^* and π_3^* in order of increasing energy. The anion states are labeled according to the virtual orbitals involved in the vertical electron attachment process. In the gas phase, the π_1^* ground state of the 1M4NI anion is bound, while π_2^* and π_3^* are resonances (unstable against auto-ionization) [42]. In the present study, the resonant character of the higher energy states is ignored, since our main interest is the solvent polarization. The excited π_2^* and π_3^* states are therefore obtained from standard electronic state techniques, which neglect the imaginary energy component associated with the auto-ionization probability. Our models also neglect the vibrational relaxation of the solute and the vibrational-orientational relaxation of the solvent arising from electron attachment. We concentrate on the polarization of the EE atomic charges, which can be viewed as the fast response to electron capture by the 1M4NI solute. The solvent response to changes in the excess charge density of the solute is also investigated, since different anion states are considered. The scPEE-S-QM/MM method is further applied to the ground and first excited states of neutral 1M4NI, to explore the solvent response to the change in the solute electronic density, and finally to neutral liquid water to assess the consistency and reliability of the methodology. Our results for liquid water are in very good agreement with the experimental data and also with recent theoretical accounts. The present applications used aqueous solvation and employed Monte Carlo method for the MM simulations to obtain solvent-solute configurations. These are not limitations of the scPEE-S-QM/MM methodology, which can be useful to more complex environments and explore molecular dynamics methods for the MM simulations, as well as other QM methods and basis sets.

2. Methods

The details of the Metropolis Monte Carlo simulations performed with the DICE software [49], selection of statistically uncorrelated configurations, and characterization of the solute-solvent hydrogen bonds by using geometrical and energetic criteria [50,51], are available in the Supporting Material (SM). The minimum distance distribution function with parallelogram normalization of $7.5\,\text{Å} \times 5.5\,\text{Å} \times 4.0\,\text{Å}$, [52] calculated from 4×10^5 Monte Carlo configurations is shown in Fig. 1 and displays three peaks. The first one, extending down to 2.2 Å, is related to the formation of 1M4NI-water hydrogen bonds and can be viewed as a microsolvation shell. Spherical integration of the minimum distance distribution function over $0 \leq r \leq 2.2\,\text{Å}$ indicates three water molecules involved in the hydrogen bonds, which is consistent with the analysis performed with 2×10^4 configurations (see the SM). The other peaks define the first and second solvation shells. They extend to 4.2 Å and 7.8 Å, respectively, and the spherical integration of the minimum distance distribution function from zero to the end of each shell indicates 36 and 155 solvent molecules. From the set of statistically uncorrelated configurations, we selected a representative configuration whose hydrogen bonds properties and vertical electron attachment energies (VAEs) are the closest to the ensemble averaged values (see the SM for details). This approach for choosing a representative configuration is based on a previous study of the microhydrated uracil [53], but here we improved the modeling of the influence of the environment by taking into account the bulk water effect on the VAEs through the EE approach. From that configuration, we also obtained the 1M4NI-$(H_2O)_3$ representative solute cluster, comprising the solute and three hydrogen-bonded water molecules.

As an initial step, prior to the scPEE-S-QM/MM procedure, the π^* anion states of the representative solute cluster, [1M4NI-$(H_2O)_3$]$^-$, were described as follows. The π_1^* bound state was computed with both the

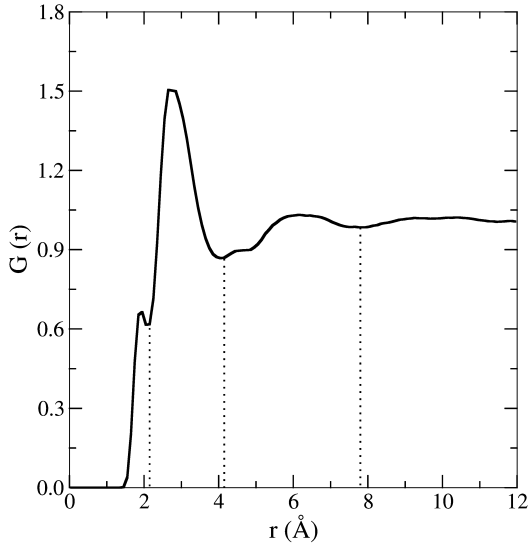

Fig. 1. Minimum distance distribution function for the solvated ground state of 1M4NI in the neutral form. The vertical lines indicate the solvation shells: up to 2.2 Å the microsolvation shell (hydrogen bonds), up to 4.2 Å the first solvation shell and up to 7.8 Å the second solvation shell.

MP2/aug-cc-pVDZ and B3LYP/6-31G* methods, whereas the anion excited states, π_2^* and π_3^*, were calculated with time-dependent density functional theory (TDDFT) employing the B3LYP [54,55] functional and the 6-31G* basis set. The solvent effects on the anion states were accounted for using the state-specific [56,57] polarizable continuum model (PCM) [58]. Atomic charges for the [1M4NI-$(H_2O)_3$]$^-$ representative solute cluster were calculated using the fitting of the QM electrostatic potential with the CHELPG method [59], independently for each π^* anion state polarized by the PCM. The structure of the 1M4NI-$(H_2O)_3$ representative solute cluster is shown in Fig. 2 along with the most important natural transition orbitals (NTOs) [60] of the $\pi_1^* \rightarrow \pi_2^*$ and $\pi_1^* \rightarrow \pi_3^*$ transitions (the π_1^* NTO is very similar in both excitations). The transitions transfer the excess charge from the nitro group (NO_2) to the ring, although more thoroughly in the $\pi_1^* \rightarrow \pi_2^*$ case. For the neutral 1M4NI-$(H_2O)_3$ representative solute cluster, the ground state was described with the MP2/aug-cc-pVDZ and B3LYP/aug-cc-pVDZ methods, while the first excited $\pi\pi^*$ singlet state was computed with TDDFT, using the B3LYP functional and the aug-cc-pVDZ basis set. The atomic charges for the neutral 1M4NI-$(H_2O)_3$ representative solute cluster were also generated with the state-specific PCM and CHELPG methods. Here, all electronic structure calculations were performed with the Gaussian09 program [61].

We now describe the scPEE-S-QM/MM method for polarization of the EE atomic charges. After generating the solute-solvent configurations from the MM simulations, subsequent QM calculations are performed on a system composed by the representative solute cluster (solute + 3 water molecules, 1M4NI-$(H_2O)_3$) and N_s solvent molecules. This QM system is initially partitioned into the explicit atomic region (wave-functions and electrons) and the polarizable EE region (only point charges), and atomic charges are recalculated for the atoms in both regions. In the present application, the initial atomic charges for the atoms of the anionic ([1M4NI-$(H_2O)_3$]$^-$) or neutral (1M4NI-$(H_2O)_3$) representative solute cluster were calculated as described above and the N_s solvent molecules were initially described with the charges of the SPC/E force field. Alternative techniques could of course be used to compute those initial charges. The solvent polarization cycle consists in performing single-molecule QM calculations to recompute the atomic charges of each solvent molecule considered in the explicit region surrounded by the polarizable EE of all other solvent and solute molecules using the precomputed atomic charges. In every step of the cycle, the atomic charges of the single solvent molecule are recalculated employing the CHELPG scheme outlined above, in the presence of the polarizable EE of the representative solute cluster and all other $N_s - 1$ solvent molecules. An iteration consists in performing N_s QM calculations (updating the atomic charges of every solvent molecule), and the solvent molecules are iterated until self-consistency is achieved, i.e., until the variations in the magnitude of the dipole moment of the solvent molecules become smaller than the convergence threshold, thus completing a solvent polarization cycle. At the end of the cycle, the atomic charges of the anionic or neutral representative solute cluster are updated therefore starting a new solvent polarization cycle. The charges of the entire system are iterated until self-consistency between successive cycles is attained, as illustrated in Fig. 3. The scPEE-S-QM/MM method shares some aspects with the SCEE model, which was recently proposed for bulk water [24] and solution [32]. However, in the SCEE method the final dipole moments, which are the same for all water molecules, are obtained with lower computational cost because only three single-molecule QM calculations are performed. In our scPEE-S-QM/MM method, each solvent molecule has individual atomic charges and dipole moment, due to the local polarization effect. In other words, each molecule is affected in a particular way by the local surroundings, a more realistic description compared to the scenario where all the molecules are affected in the same way. Of course, that the scPEE-S-QM/MM method involves a higher computational cost because several single-molecule QM calculations are performed in each polarization cycle. As discussed below (see details in SM), typically four iterations are necessary to obtain converged dipole moments for the solvent molecules.

The scPEE-S-QM/MM scheme was applied for the representative configuration, comprising by the representative solute cluster in the anionic ([1M4NI-$(H_2O)_3$]$^-$) and neutral (1M4NI-$(H_2O)_3$) forms surrounded by 500 water molecules. The solvent polarization steps were carried out by treating the individual water molecules at the MP2/6-31G* level. For each solvent molecule, the dipole moment was considered converged for $\Delta\mu_i < 10^{-4}$ D, where $\Delta\mu_i$ is the variation of the dipole moment between successive polarization iterations. For the solute representative cluster, the convergence criterion was $\Delta q_k < 10^{-4}$ a.u., where Δq_k is the charge variation of the k-th atom between successive polarization cycles.

3. Results and discussion

The converged charges and dipole moment values for the 500 water molecules of the polarized EE are shown in Figs. 4 and 5, respectively. The calculations considered the ground (π_1^*) and excited (π_2^* and π_3^*) anion states, as indicated by the color code. As reference values, we obtained atomic charges ($q_O = -0.8579$ a.u. and $q_H = 0.4278$ a.u.) and the dipole moment (2.3247 D) for a single water molecule in PCM environment, using the MP2/6-31G* and CHELPG methods. Those reference values are shown as horizontal dashed lines in Figs. 4 and 5. For each water molecule, H1 and H2 are, respectively, the closer and further lying hydrogen atoms with respect to the solute, as defined by the minimum distance to the 1M4NI anion. The polarization of the atoms in the polarized EE region (Fig. 4) is sensitive to the electronic state of the anionic explicit region within and around the first solvation shell ($\lesssim 4$ Å), but not for larger distances. For ≈ 406 water molecules out of 500 (81%), the converged charges are larger in absolute value than the water-in-PCM reference values. For ≈ 94 molecules (19%), the self consistent charges are smaller than the reference for at least one atom, which can be viewed as a vacuum effect, i.e., an artifact of the finite-sized system employed in the calculations. This effect is mainly observed for molecules lying far from the solute, beyond 10.9 Å, as indicated by the vertical lines in Figs. 4 and 5.

The converged dipole moments, shown as a function of the minimum distance to the anion solute in the upper panel of Fig. 5, behave similarly as the atomic charges. The converged values significantly depend on the electronic states within and around the first solvation shell,

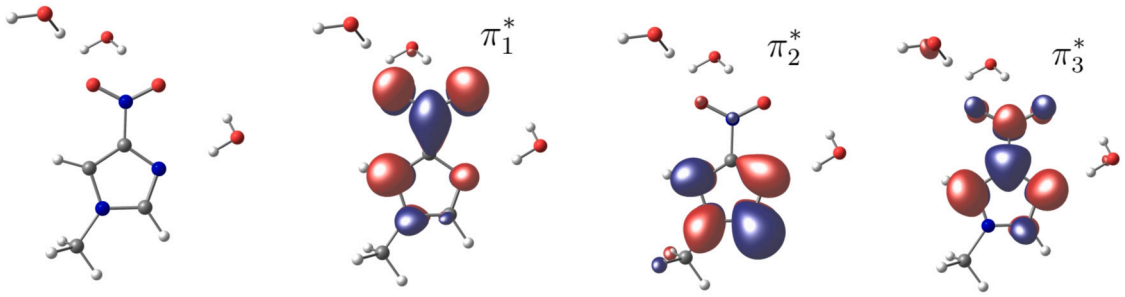

Fig. 2. Structure of the representative cluster, 1M4NI-$(H_2O)_3$. The oxygen and the rightmost nitrogen atoms of the solute act as acceptors in the Hydrogen bonds. Natural transition orbitals representing $\pi_1^* \rightarrow \pi_2^*$ and $\pi_1^* \rightarrow \pi_3^*$ excitations are also shown.

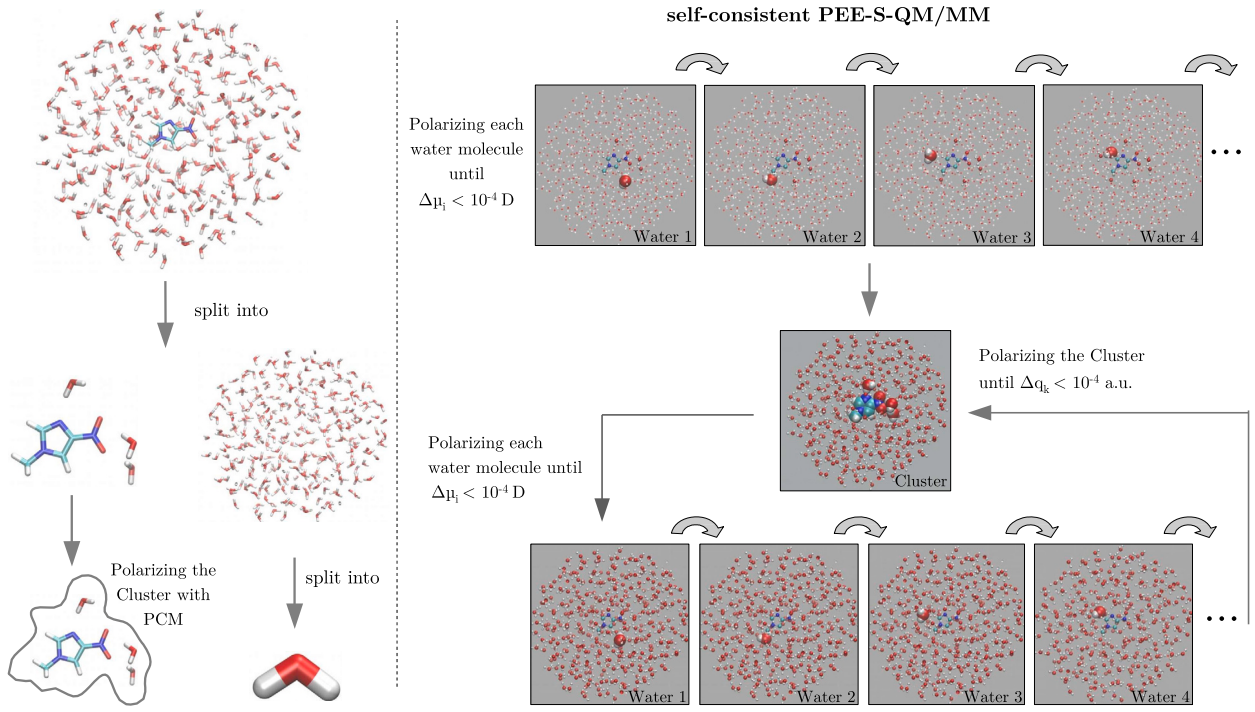

Fig. 3. Depiction of the scPEE-S-QM/MM method. The initial stages are represented in the left panel: The system is partitioned into a representative solute cluster (1M4NI-$(H_2O)_3$) and N_s individual water molecules. Initial atomic charges are computed for the representative solute cluster in the explicit region, with the solvent described by the polarizable continuum model, PCM, and for the solvent molecules they are initially considered as the SPC/E force field atomic charges. Then, the scPEE-S-QM/MM cycle starts (represented in the right panel): The atomic charges of each solvent molecule are recalculated at the QM level in the presence of the polarizable EE composed by the solute representative cluster and all other solvent molecules. Once the atomic charges of all solvent molecule have been recalculated, an iteration step is completed. The solvent subsystem is iterated until self-consistency is achieved, thus completing one solvent polarization cycle. At the end of the cycle, the atomic charges of the solute representative cluster are recalculated, and a new solvent polarization cycle is performed. The procedure is terminated after attaining self-consistency between successive cycles. All charges calculations are performed with the CHELPG method at QM level. In the image, the molecule (or cluster) that is being polarized in explicit region of the QM calculation is shown with the van der Waals (VDW) representation surrounded by the polarizable EE of remaining molecules. The molecules, which have been polarized, are shown with the Corey-Puling-Koltun (CPK) representation, while those ones not yet polarized are represented by point charges.

and the vacuum effect reflecting the finite size of the system is also evident. The dipole moments exceed the reference value (horizontal line) for ≈ 466 water molecules (93%), although for another ≈ 34 molecules (7%) some dipole moments drop below the reference. The same behavior is observed in the lower panel of Fig. 5, which shows the dependence of the dipole moments with respect to the distance between the centers of mass of the solvent and solute molecules (in this case, the vacuum effect is found beyond 12.8 Å). Despite the finite-size artifact, both the charges and dipole moments point out a remarkable long-ranged polarization effect. While one could expect the polarization intensity to decrease as a function of the distance to the solute, such trend is not clear for $R \lesssim 11$ Å (onset of the vacuum effect). At any distance, the atomic charge and dipole moment values spread considerably, although often exceeding the water-in-PCM references in absolute value. Each water molecule is polarized by the anionic representative solute cluster and also by the surrounding water molecules. The polarization strength does not simply depend on the solvent-solute distance. It also has a local character which causes the charges and dipole moments to fluctuate considerably among molecules lying at similar distances from the solute.

The distribution of the dipole moments of water molecules obtained for the neutral representative solute cluster, 1M4NI-$(H_2O)_3$, is shown in Figs. S5 and S6. The dipole moments and the atomic charges (not shown) have similar features as those computed for the anionic representative solute cluster. The local effect is also very clear as the dipole moments fluctuate considerably for water molecules lying at similar distances from the solute. The converged values exceed the water-in-PCM reference value, although the finite-size artifact becomes clear around

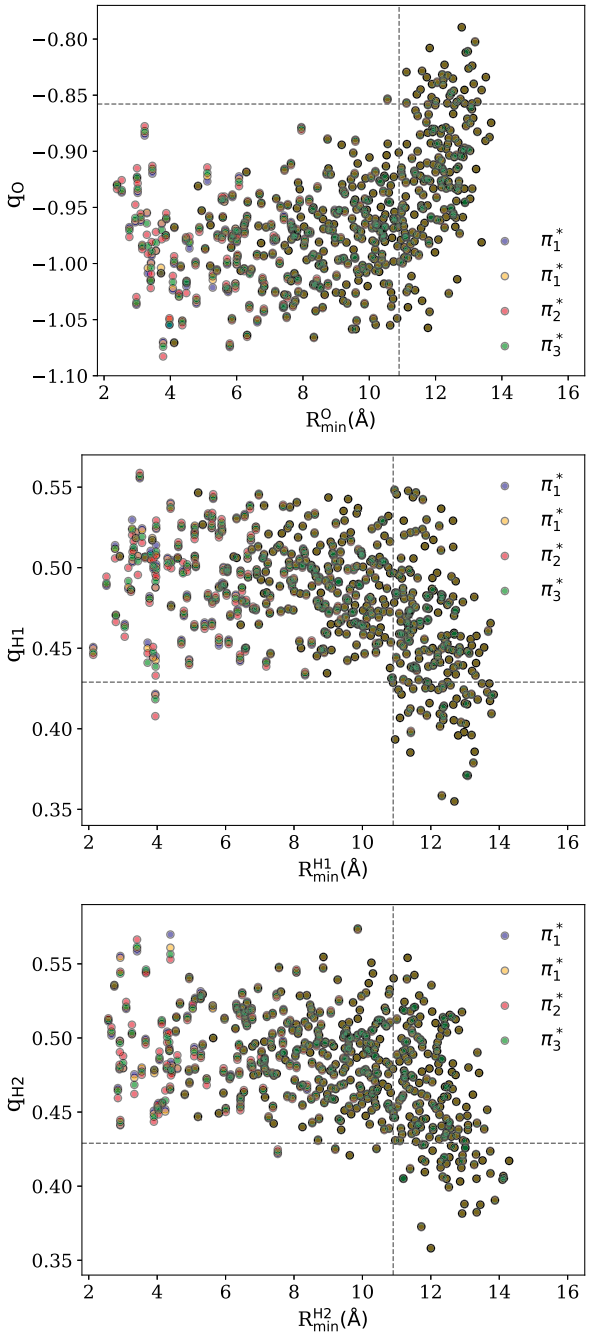

Fig. 4. Converged atomic charges (in atomic units) for the 500 water molecules polarized by different electronic states of the $[1M4NI\text{-}(H_2O)_3]^-$ cluster: π_1^* (blue: MP2/aug-cc-pVDZ, yellow: B3LYP/6-31G*), π_2^* (red: B3LYP/6-31G*) and π_3^* (green: B3LYP/6-31G*). The charges are indicated as q_O for the oxygen atom, as well as q_{H1} and q_{H2} for the hydrogen atoms, where H1 lies closer to the solute based on the minimum distance (R_{min}). The horizontal lines correspond to the water-in-PCM reference values, while the vertical lines (10.9 Å) indicate the onset of the vacuum effect (artifact arising from the finite size of the system).

11 Å (minimum distances). The dipole moments of the water molecules polarized by the ground state of the $1M4NI\text{-}(H_2O)_3$ (n) can be distinguished from those polarized by the three π^* anion states over the entire 11-Å range, as the n points are generally not superimposed with the π^* ones in Fig. S5. The comparison between the dipole moments of water molecules calculated for the ground (n) and excited ($\pi\pi^*$) states of the neutral represetantive solute cluster are quite distinguishable only within and around the first solvation shell (Fig. S6).

Table 1
Average values and statistical errors (the latter in parentheses) for the atomic charges (in atomic units) and dipole moment (in Debye) of the water molecules polarized by different π^* electronic states of anionic representative solute cluster, $[1M4NI\text{-}(H_2O)_3]^-$, and by the ground n and excited $\pi\pi^*$ electronic states of neutral representative solute cluster, $1M4NI\text{-}(H_2O)_3$, using scPEE-S-QM/MM method. The pure water polarization is also shown for comparison considering the solvent environment as PCM and as the electrostatic embedding EE of the water force field, SPC/E.

System in water	q_O	q_{H1}	q_{H2}	μ_L
Anionic solute cluster (π_1^*, π_2^* and π_3^*)	−0.985(3)	0.494(2)	0.491(2)	2.69(1)
Neutral solute cluster (n and $\pi\pi^*$)	−0.985(3)	0.493(2)	0.491(2)	2.69(1)
Water (PCM)	−0.8579	0.4289	0.4289	2.3247
Water (EE = SPC/E)	−0.8476	0.4238	0.4238	2.3512

The average values and statistical errors for the atomic charges and dipole moments of water molecules, computed for the anionic and neutral representative solute cluster, are shown in Table 1. To avoid the finite-size artifact, we only considered the molecules lying in the first and second solvation shells, corresponding to $R_{min} \lesssim 7.8$ Å (details of the statistical analysis are given as SM, see Tab. S2 and Fig. S4). The average values of atomic charges and dipole moments of water molecules obtained for the anionic representative solute cluster in its different π^* states converged essentially to the same value (see Table 1). The correspondent values for the n and $\pi\pi^*$ states of the neutral representative solute cluster also converged to the same value (see Table 1). The small statistical errors indicate reasonably well converged average values, which are essentially identical for the neutral and anionic representative solute cluster and ≈ 15% larger in magnitude than the SPC/E and water-in-PCM counterparts. Deeper insight into the convergence can be gained from Fig. 6 where the average dipole moments are computed as a function of the distance to the solvent, gradually increasing the number of water molecules considered in the calculations (total of 155 molecules). Around the first solvation shell, the average values obtained for the π^* anion states and the neutral ground state differ among each other, despite the considerable statistical errors. Around and beyond the second solvation shell, the dipole moments converge, which is consistent with the distributions shown in Figs. 4, 5, and Fig. S5.

While the average atomic charges and dipole moments of the solvent molecules are insensitive to the charge and electronic state of the representative solute cluster for a sufficiently large collection of water molecules, the polarization seems to be state- and charge-specific within the first solvation shell. We therefore investigated the dependence of some electronic properties of the neutral representative solute cluster with respect to the polarization of the solvent. To keep the discussion concise, we considered the energies of the molecular orbitals relevant to the electronic states of the neutral and anionic representative solute cluster. Specifically, we computed the energies of the π_1 (HOMO), π_1^* (LUMO), π_2^* and π_3^* virtual orbitals, and the dipole moment for $1M4NI\text{-}(H_2O)_3$ at the Hartree-Fock (HF)/6-31G* level, and also the energy of the π_1^* (SOMO) for $[1M4NI\text{-}(H_2O)_3]^-$, employing the unrestricted HF method and the 6-31+G* basis set. The calculations were performed for the representative configuration including 155 solvent molecules in the EE region, which comprise to the first and second solvation shells. The orbital energies and the dipole moment were computed with different polarization strategies for the EE partition. We considered the average atomic charges given in Table 1, the specific scPEE-S-QM/MM atomic charges obtained for the n, $\pi\pi^*$, π_1^*, π_2^*, and π_3^* states, and also the SPC/E charges for comparison.

As shown in Table 2, the orbital energies significantly depend on the EE atomic charges, with variations around and above 0.5 eV. Although the dipole moment of the neutral representative solute cluster is less sensitive to the solvent polarization, the discrepancies can be as large as 0.4 D. In general, the energies obtained with the scPEE-S-QM/MM atomic charges for the n state are fairly close to those computed with the scPEE-S-QM/MM-$\pi\pi^*$ atomic charges (discrepancies of 0.01 eV to

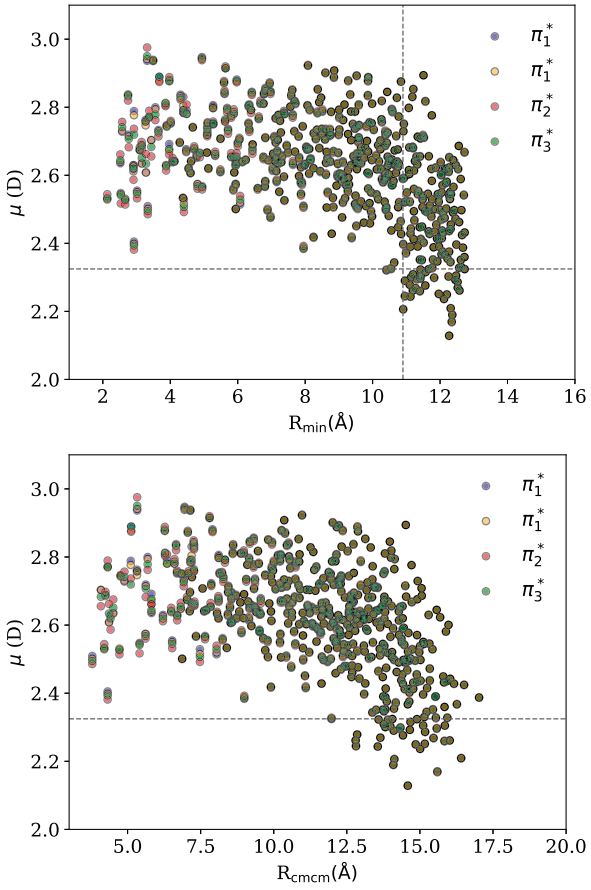

Fig. 5. Converged dipole moments (μ) for the 500 water molecules polarized by different electronic states of the $[1M4NI\text{-}(H_2O)_3]^-$ cluster: π_1^* (blue: MP2/aug-cc-pVDZ, yellow: B3LYP/6-31G*), π_2^* (red: B3LYP/6-31G*) and π_3^* (green: B3LYP/6-31G*). The dipole moment is shown as a function of the minimum distance to the solute (R_{min}, upper panel) and the distance between the centers of mass of the solute and the water molecules (R_{cmcm}, lower panel). The horizontal lines correspond to the water-in-PCM reference values, while the vertical line (10.9 Å) indicates the onset of the vacuum effect (artifact arising from the finite size of the system).

0.03 eV), SPC/E atomic charges (discrepancies of 0.05 eV to 0.10 eV) and the average atomic charges (discrepancies of 0.10 eV to 0.14 eV). There is also good agreement for the energies computed with the scPEE-S-QM/MM atomic charges converged for the π^* anion states. However, the energies are charge-sensitive, i.e., the solvent molecules in the EE region polarized by the neutral and anionic representative solute cluster produce significantly distinct results. The π^* orbital energies of the neutral representative solute cluster can be viewed as approximations to the resonance energies, according to Koopman's theorem. In case electronic polarization in the explicit region comprising the representative solute cluster was accounted for in those energy estimates, the stabilization of the π^* resonances induced by the molecules in the polarizable EE region would be more significant. Interestingly, the HOMO-LUMO gap is barely affected by the polarization scheme since the orbitals show similar energy shifts.

Crucial aspects regarding the computational demand of the scPEE-S-QM/MM method are the number of polarization cycles and the number of iterations in each cycle. The convergence of the charges and dipole moments of the solvent molecules from the polarizable EE region in the first cycle is illustrated in the SM in Figs. S7, S8, S9, and S10. It is evident that the most of the polarization is already accounted for with 2-4 iterations, suggesting that the convergence thresholds could be loosened. While we did not perform a systematic investigation of the numerical parameters, we found that only a single polarization cycle

Table 2
The energies (in eV) of the π_1, π_1^*, π_2^*, and π_3^* orbitals and the dipole moment (in Debye) of the neutral representative solute cluster, 1M4NI-$(H_2O)_3$, and the energy of the SOMO π_1^* of the anionic representative solute cluster calculated with different polarized electrostatic embedding PEE generated with scPEE-S-QM/MM charges using an average polarization for all solvent molecules and the individual polarization of each solvent molecule with the neutral representative solute cluster at the ground n and excited $\pi\pi^*$ electronic states and also at the three π^* states of the anionic representative solute cluster (π_1^*, π_2^* and π_3^*). The results calculated with the electrostatic embedding EE of the water force field, SPC/E, are also shown for comparison.

Solute cluster state	Neutral					Anion
Average polarization	π_1	π_1^*	π_2^*	π_3^*	μ	SOMO (π_1^*)
Neutral/Anionic	−9.96	1.10	4.13	6.06	16.68	−2.93
EE = SPC/E	−10.02	1.09	4.04	6.02	16.32	−2.92
Individual polarization	π_1	π_1^*	π_2^*	π_3^*	μ	SOMO (π_1^*)
Neutral ground n	−10.08	1.00	3.99	5.95	16.66	−3.02
Neutral excited $\pi\pi^*$	−10.06	0.99	4.02	5.94	16.72	−3.04
Anionic π_1^*	−10.49	0.57	3.60	5.55	16.75	−3.46
Anionic π_2^*	−10.50	0.60	3.57	5.55	16.65	−3.41
Anionic π_3^*	−10.49	0.59	3.59	5.56	16.72	−3.43

Table 3
Average values and statistical errors (the latter in parentheses) for the atomic charges (in atomic units) and dipole moment (in Debye) for a water molecule polarized by pure liquid water, computed at different levels of calculation. The reference for water-in-PCM and the SPC/E models are also shown.

Method	q_O	q_{H1}	q_{H2}	μ_L
MP2/6-31G*	−1.003(4)	0.499(2)	0.504(2)	2.74(1)
MP2/aug-cc-pVDZ	−0.994(5)	0.493(3)	0.501(3)	2.75(2)
MP2/aug-cc-pVTZ	−1.017(6)	0.504(3)	0.513(3)	2.81(2)
MP2/aug-cc-pVQZ	−1.027(6)	0.509(3)	0.518(4)	2.84(2)
B3LYP/aug-cc-pVTZ	−1.015(6)	0.503(3)	0.512(3)	2.81(2)
Reference	−0.8579	0.4289	0.4289	2.3247
SPC/E	−0.8476	0.4238	0.4238	2.3512

was necessary. In practice, obtaining the atomic charges for the explicit atoms of the representative solute cluster in PCM environment and performing a single solvent polarization cycle for the solvent molecules in the polarizable EE region provided essentially the same results as those presented in Tables 1 and 2, which required 4 to 9 cycles for the different charges and electronic states of the representative solute cluster employing the convergence criteria described before. Results obtained for an additional solute-solvent configuration can be seen in the SM (see Figs. S11, S12, S13, S14 and S15).

As an additional application of the scPEE-S-QM/MM method, we investigated the properties of liquid water. The average values of the dipole moment and atomic charges of a water molecule polarized by the polarizable EE water environment are given in Table 3. The dipole moments of liquid water, computed with different quantum chemistry methods to update the atomic charges, range from 2.74(1) D to 2.84(2) D. The results correspond to ensemble averages performed with 86 statistically uncorrelated Monte Carlo configurations (see the SM for details) and generally agree with previous accounts [20,24,62–76] which reported values between 2.4 D and 3.1 D. Our best estimates were 2.81(2) D, which was obtained with both the B3LYP/aug-cc-pVTZ and MP2/aug-cc-pVTZ methods, and also 2.84(2) D, calculated at the MP2/aug-cc-pVQZ level. These results are in very good agreement with the experimental value of 2.9(6) D [77], and also with recently reported calculations, 2.72(2) D to 2.83(2) D [24], and also ≈ 2.85 D [76]. Details of our calculations are given as SM (see Figs. S17, S18, S19, S20, S21, S22, S23, S24, S25 and also Tab. S3).

We also computed the induced dipole moment, $\Delta\mu$, defined as the difference between the dipole moments of the water molecule in the liquid and gas phases, as shown in Table 4. For liquid water, we

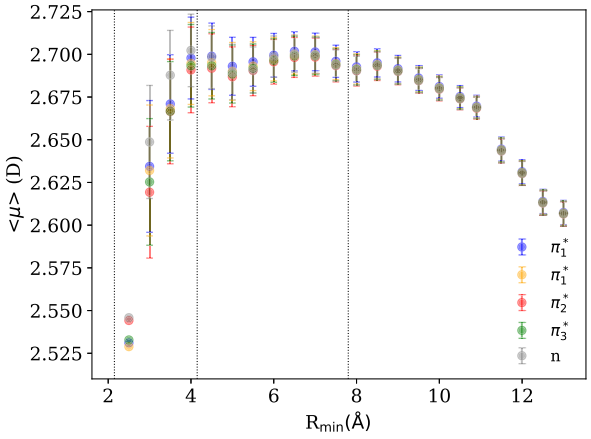

Fig. 6. Average values of the dipole moments of the water molecules ($\langle\mu\rangle$) are shown as a function of the minimum distance, so the number of molecules included in the calculation gradually increases. The results are shown for the different electronic states of the aionic solute cluster $[1M4NI\text{-}(H_2O)_3]^-$: π_1^* (blue: MP2/aug-cc-pVDZ, yellow: B3LYP/6-31G*), π_2^* (red: B3LYP/6-31G*) and π_3^* (green: B3LYP/6-31G*), and the ground state (n) of the neutral solute cluster, $1M4NI\text{-}(H_2O)_3$ (gray: MP2/aug-cc-pVDZ). The vertical lines indicate the solvation shells, and the error bars correspond to the statistical errors.

Table 4
Induced dipole moment ($\Delta\mu$) computed as the difference between the dipole moments of the water molecule in the liquid (μ_L) and gas (μ_G) phases, at different levels of calculation. The liquid-phase (μ_L^{corr}) and induced ($\Delta\mu^{corr}$) dipole moments were also corrected to account for geometry relaxation (see text).

	μ_G	μ_L	μ_L^{corr}	$\Delta\mu$	$\Delta\mu^{corr}$
MP2/6-31G*	2.20	2.74(1)	2.82(1)	0.54(1)	0.62(1)
MP2/aug-cc-pVDZ	1.88	2.75(2)	2.83(2)	0.87(2)	0.95(2)
MP2/aug-cc-pVTZ	1.86	2.81(2)	2.89(2)	0.95(2)	1.03(2)
MP2/aug-cc-pVQZ	1.86	2.84(2)	2.92(2)	0.98(2)	1.06(2)
B3LYP/aug-cc-pVTZ	1.85	2.81(2)	2.89(2)	0.96(2)	1.04(2)
Exp.	1.855 [78]	2.9(6) [77]	–	~ 1.05	–

used the SPC/E geometry, while the water in the gas phase had its geometry optimized. Our calculations, performed with the SPC/E geometry, were corrected to account for geometry relaxation, employing the 0.08 D shift recommended by Jorge *et al.* [24]. Our $\Delta\mu$ results range between 0.54(1) D and 0.98(2) D, depending on the calculation method. These estimates are consistent with other calculations [20,24,62–65,68–70,72], with reported values around 0.44 D to 1.1 D. Our best results are 0.95(2) D (MP2/aug-cc-pVTZ), 0.96(2) D (B3LYP/aug-cc-pVTZ) and 0.98(2) D (MP2/aug-cc-pVQZ), which can be corrected to 1.03(2) D, 1.04(2) D and 1.06(2) D, respectively, accounting for geometry relaxation. These results are in excellent agreement with a recent theoretical account [24], which predicted induced dipole moments between 0.87(2) D and 0.97(2) D, and also with the experimental value of 1.05 D, estimated as the difference between the experimental data for the liquid (2.9(6) D) [77] and the gas phase (1.855 D) [78]. The agreement with experiment for the induced dipole is not coincidental, as our best calculations for the liquid and the gas also agree very well with the data. The quality of our results for liquid water further corroborate scPEE-S-QM/MM as an attractive alternative to account for the polarization of the electrostatic embedding.

4. Conclusions

In conclusion, we proposed the scPEE-S-QM/MM methodology to account for mutual polarization in the S-QM/MM framework. The first applications concerned the ground and excited states of $1M4NI\text{-}(H_2O)_3$ cluster, in the neutral and anion forms. Our results point out a significant local polarization effect. Even for the anion solute, the polarization strength of the polarizable EE region does not show a clear dependence on the distance from the solute over 11 Å. At any given distance within this range, the atomic charges and dipole moment of the solvent molecules spread considerably pointing out the influence of the neighboring solvent molecules. For both the anion and neutral solutes, the polarized atomic charges of the polarizable EE region are sensitive to the electronic state of the cluster only within and around the first solvation shell. For larger distances the polarized EE atomic charges are not sensitive to the state of the cluster, only to its charge. In particular, the average polarized EE atomic charges obtained for two states of the neutral solute cluster (n and $\pi\pi^*$) are essentially identical to the average values obtained for three π^* states of the anion species. The average values were found to exceed in magnitude the SPC/E and water-in-PCM charges by ≈ 15%. Electronic properties of the $1M4NI\text{-}(H_2O)_3$ and $[1M4NI\text{-}(H_2O)_3]^-$ clusters were investigated under the influence of different polarized embeddings. The polarized EE atomic charges obtained from different electronic states of the neutral species provided similar results, and the same was found for the electronic states of the anion. However, the EE atomic charges polarized by the $1M4NI\text{-}(H_2O)_3$ and $[1M4NI\text{-}(H_2O)_3]^-$ clusters produced significantly distinct results for the orbital energies of the $1M4NI\text{-}(H_2O)_3$, i.e., the polarization was found to be charge-sensitive. In comparison with the SPC/E result, the different polarized EE atomic charges (average or specific) impacted the dipole moment of the $1M4NI\text{-}(H_2O)_3$. Interestingly, the HOMO-LUMO gap was barely affected by the different polarized embeddings since the orbitals had similar energy shifts.

The scPEE-S-QM/MM method was also employed to investigate the properties of pure liquid water. The dipole moment of the water molecule in liquid phase, as well as its difference with respect to the gas-phase dipole moment, are in very good agreement with the experimental data and also with recent theoretical accounts, thus showing the consistency and reliability of the scPEE-S-QM/MM method.

5. List of acronyms

1M4NI 1-methyl-4-nitroimidazole
CHELPG CHarges from ELectrostatic Potentials using a Grid-based method
EE Electrostatic Embedding
HOMO Highest Occupied Molecular Orbital
LUMO Lowest Unoccupied Molecular Orbital
MM Molecular Mechanics
MP2 Moller-Plesset 2nd order perturbation
NTO Natural Transition Orbital
PCM Polarizable Continuum Model
PE Polarized Embedding
QM Quantum Mechanics
scPEE Self-Consistent Polarizable Electrostatic Embedding
SM Supporting Material
SOMO Singly Occupied Molecular Orbital
S-QM/MM Sequential Hybrid QM/MM method
TDDFT Time-Dependent Density Functional Theory
VAE Vertical Electron Attachment Energy

Declaration of competing interest

The authors declare that they have no known competing financial interests or personal relationships that could have appeared to influence the work reported in this paper.

Data availability

Data will be made available on request.

Acknowledgement

M.B.K. acknowledges financial support (CNPq) (grant No. 142103/2019-5). M.T. do N.V. also acknowledges financial support (CNPq) (grant No. 304571/2018-0) and FAPESP (grant No. 2020/16155-7). K.C. acknowledges financial support FAPESP (grant 2021/09016-3). The calculations were partly performed with HPC resources from STI, University of São Paulo.

Appendix A. Supplementary material

Supplementary material related to this article can be found online at https://doi.org/10.1016/j.molliq.2023.122861.

References

[1] A. Warshel, M. Levitt, Theoretical studies of enzymic reactions: dielectric, electrostatic and steric stabilization of the carbonium ion in the reaction of lysozyme, J. Mol. Biol. 103 (1976) 227–249.
[2] H.M. Senn, W. Thiel, QM/MM methods for biomolecular systems, Angew. Chem., Int. Ed. Engl. 48 (2009) 1198–1229.
[3] M.W. van der Kamp, A.J. Mulholland, Combined quantum mechanics/molecular mechanics (QM/MM) methods in computational enzymology, Biochemistry 52 (2013) 2708–2728.
[4] M. Liu, Y. Wang, Y. Chen, M.J. Field, J. Gao, QM/MM through the 1990s: the first twenty years of method development and applications, Isr. J. Chem. 54 (2014) 1250–1263.
[5] U.N. Morzan, D.J. Alonso de Armiño, N.O. Foglia, F. Ramírez, M.C. González Lebrero, D.A. Scherlis, D.A. Estrin, Spectroscopy in complex environments from QM–MM simulations, Chem. Rev. 118 (2018) 4071–4113.
[6] T. Andruniów, M. Olivucci, QM/MM Studies of Light-Responsive Biological Systems, Springer, 2021.
[7] H.M. Senn, W. Thiel, in: M. Reiher (Ed.), Atomistic Approaches in Modern Biology: From Quantum Chemistry to Molecular Simulations, Springer Berlin Heidelberg, Berlin, Heidelberg, 2007, pp. 173–290.
[8] J.-L. Rivail, M. Ruiz-Lopez, X. Assfeld, Quantum Modeling of Complex Molecular Systems, vol. 21, Springer, 2015.
[9] R.P. Magalhães, H.S. Fernandes, S.F. Sousa, Modelling enzymatic mechanisms with QM/MM approaches: current status and future challenges, Isr. J. Chem. 60 (2020) 655–666.
[10] J. Nochebuena, S. Naseem-Khan, G.A. Cisneros, Development and application of quantum mechanics/molecular mechanics methods with advanced polarizable potentials, WIREs Comput. Mol. Sci. 11 (2021) e1515.
[11] K. Coutinho, S. Canuto, in: P.-O. Löwdin, J.R. Sabin, M.C. Zerner, J. Karwowski, M. Karelson (Eds.), Solvent Effects from a Sequential Monte Carlo - Quantum Mechanical Approach, in: Advances in Quantum Chemistry, vol. 28, Academic Press, 1997, pp. 89–105.
[12] K. Coutinho, S. Canuto, M.C. Zerner, A Monte Carlo-quantum mechanics study of the solvatochromic shifts of the lowest transition of benzene, J. Chem. Phys. 112 (2000) 9874–9880.
[13] Y. Tu, A. Laaksonen, The electronic properties of water molecules in water clusters and liquid water, Chem. Phys. Lett. 329 (2000) 283–288.
[14] L. Cao, U. Ryde, On the difference between additive and subtractive QM/MM calculations, Front. Chem. 6 (2018).
[15] M.R. Provorse, T. Peev, C. Xiong, C.M. Isborn, Correction to “convergence of excitation energies in mixed quantum and classical solvent: comparison of continuum and point charge models”, J. Phys. Chem. B 121 (2017) 2372.
[16] J.M. Milanese, M.R. Provorse, E. Alameda, C.M. Isborn, Convergence of computed aqueous absorption spectra with explicit quantum mechanical solvent, J. Chem. Theory Comput. 13 (2017) 2159–2171.
[17] Y. Zhang, J. Wang, S. Yang, Notable effect of water on excess electron attachment to aqueous DNA deoxyribonucleosides, Phys. Chem. Chem. Phys. 21 (2019) 8925–8932.
[18] M.A. Thompson, G.K. Schenter, Excited states of the bacteriochlorophyll b dimer of rhodopseudomonas viridis: a QM/MM study of the photosynthetic reaction center that includes MM polarization, J. Phys. Chem. 99 (1995) 6374–6386.
[19] D. Loco, E. Polack, S. Caprasecca, L. Lagardère, F. Lipparini, J.-P. Piquemal, B. Mennucci, A QM/MM approach using the AMOEBA polarizable embedding: from ground state energies to electronic excitations, J. Chem. Theory Comput. 12 (2016) 3654–3661.
[20] S.W. Rick, S.J. Stuart, B.J. Berne, Dynamical fluctuating charge force fields: application to liquid water, J. Chem. Phys. 101 (1994) 6141–6156.
[21] F. Lipparini, V. Barone, Polarizable force fields and polarizable continuum model: a fluctuating charges/PCM approach. 1. Theory and implementation, J. Chem. Theory Comput. 7 (2011) 3711–3724.
[22] G. Lamoureux, A.D. MacKerell, B. Roux, A simple polarizable model of water based on classical Drude oscillators, J. Chem. Phys. 119 (2003) 5185–5197.
[23] E. Boulanger, W. Thiel, Solvent boundary potentials for hybrid QM/MM computations using classical Drude oscillators: a fully polarizable model, J. Chem. Theory Comput. 8 (2012) 4527–4538.
[24] M. Jorge, J.R. Gomes, A.W. Milne, Self-consistent electrostatic embedding for liquid phase polarization, J. Mol. Liq. 322 (2021) 114550.
[25] M. Mukherjee, D. Tripathi, M. Brehm, C. Riplinger, A.K. Dutta, Efficient EOM-CC-based protocol for the calculation of electron affinity of solvated nucleobases: uracil as a case study, J. Chem. Theory Comput. 17 (2021) 105–116.
[26] J. Kongsted, A. Osted, K.V. Mikkelsen, P.-O. Åstrand, O. Christiansen, Solvent effects on the $n \rightarrow \pi^*$ electronic transition in formaldehyde: a combined coupled cluster/molecular dynamics study, J. Chem. Phys. 121 (2004) 8435–8445.
[27] H.C. Georg, K. Coutinho, S. Canuto, Converged electronic polarization of acetone in liquid water and the role in the $n - \pi^*$ transition, Chem. Phys. Lett. 429 (2006) 119–123.
[28] V. Manzoni, M.L. Lyra, R.M. Gester, K. Coutinho, S. Canuto, Study of the optical and magnetic properties of pyrimidine in water combining PCM and QM/MM methodologies, Phys. Chem. Chem. Phys. 12 (2010) 14023–14033.
[29] C.C. Vequi-Suplicy, K. Coutinho, M.T. Lamy, Electric dipole moments of the fluorescent probes Prodan and Laurdan: experimental and theoretical evaluations, Biophys. Rev. 6 (2014) 63–74.
[30] A new interpretation of the absorption and the dual fluorescence of Prodan in solution, J. Chem. Phys. 153 (2020) 244104.
[31] J.L. Silva, I. Unger, T.A. Matias, L.R. Franco, G. Damas, L.T. Costa, K.C.F. Toledo, T.C.R. Rocha, A.N. de Brito, C.-M. Saak, K. Coutinho, K. Araki, O. Björneholm, B. Brena, C.M. Araujo, X-ray photoelectron fingerprints of high-valence ruthenium–oxo complexes along the oxidation reaction pathway in an aqueous environment, J. Phys. Chem. Lett. 10 (2019) 7636–7643, PMID: 31747290.
[32] The dipole moment of alcohols in the liquid phase and in solution, J. Mol. Liq. 356 (2022) 119033.
[33] B. Boudaïffa, P. Cloutier, D. Hunting, M.A. Huels, L. Sanche, Resonant formation of DNA strand breaks by low-energy (3 to 20 eV) electrons, Science 287 (2000) 1658–1660.
[34] F. Martin, P.D. Burrow, Z. Cai, P. Cloutier, D. Hunting, L. Sanche, DNA strand breaks induced by 0-4 eV electrons: the role of shape resonances, Phys. Rev. Lett. 93 (2004) 068101.
[35] E. Alizadeh, L. Sanche, Precursors of solvated electrons in radiobiological physics and chemistry, Chem. Rev. 112 (2012) 5578–5602.
[36] E. Alizadeh, T.M. Orlando, L. Sanche, Biomolecular damage induced by ionizing radiation: the direct and indirect effects of low-energy electrons on DNA, Annu. Rev. Phys. Chem. 66 (2015) 379–398.
[37] J. Kohanoff, M. McAllister, G.A. Tribello, B. Gu, Interactions between low energy electrons and DNA: a perspective from first-principles simulations, J. Phys. Condens. Matter 29 (2017) 383001.
[38] P. Wardman, Chemical radiosensitizers for use in radiotherapy, Clin. Oncol. 19 (2007) 397–417, Importance of Radiobiology to Cancer Therapy: Current Practice and Future Perspectives.
[39] R. Schürmann, S. Vogel, K. Ebel, I. Bald, The physico-chemical basis of DNA radiosensitization: implications for cancer radiation therapy, Chem. Eur. J. 24 (2018) 10271–10279.
[40] K. Tanzer, L. Feketeová, B. Puschnigg, P. Scheier, E. Illenberger, S. Denifl, Reactions in nitroimidazole triggered by low-energy (0–2 eV) electrons: methylation at N1-H completely blocks reactivity, Angew. Chem., Int. Ed. Engl. 53 (2014) 12240–12243.
[41] K. Tanzer, L. Feketeová, B. Puschnigg, P. Scheier, E. Illenberger, S. Denifl, Reactions in nitroimidazole and methylnitroimidazole triggered by low-energy (0–8 eV) electrons, J. Phys. Chem. A 119 (2015) 6668–6675.
[42] F. Kossoski, M.T. d. N. Varella, How does methylation suppress the electron-induced decomposition of 1-methyl-nitroimidazoles?, J. Chem. Phys. 147 (2017) 164310.
[43] A. Ribar, K. Fink, M. Probst, S.E. Huber, L. Feketeová, S. Denifl, Isomer selectivity in low-energy electron attachment to nitroimidazoles, Chem. Eur. J. 23 (2017) 12892–12899.
[44] R. Meißner, L. Feketeová, E. Illenberger, S. Denifl, Reactions in the radiosensitizer misonidazole induced by low-energy (0–10 eV) electrons, Int. J. Mol. Sci. 20 (2019).
[45] M. Mendes, M. Probst, T. Maihom, G. García, P. Limão-Vieira, Selective bond excision in nitroimidazoles by electron transfer experiments, J. Phys. Chem. A 123 (2019) 4068–4073.
[46] M. Mendes, G. García, M.-C. Bacchus-Montabonel, P. Limão-Vieira, Electron transfer induced decomposition in potassium–nitroimidazoles collisions: an experimental and theoretical work, Int. J. Mol. Sci. 20 (2019).
[47] M. Ončák, R. Meißner, E. Arthur-Baidoo, S. Denifl, T.F.M. Luxford, A. Pysanenko, M. Fárník, J. Pinkas, J. Kočišek, Ring formation and hydration effects in electron attachment to misonidazole, Int. J. Mol. Sci. 20 (2019).
[48] R. Meißner, J. Kočišek, L. Feketeová, J. Fedor, M. Fárník, P. Limão-Vieira, E. Illenberger, S. Denifl, Low-energy electrons transform the nimorazole molecule into a radiosensitiser, Nat. Commun. 10 (2019) 2388.
[49] H.M. Cezar, S. Canuto, K. Coutinho, Solvent effect on the syn/anti conformational stability: a comparison between conformational bias Monte Carlo and molecular dynamics methods, Int. J. Quant. Chem. 119 (2019) e25688.
[50] M.V.A. Damasceno, B.J. Costa Cabral, K. Coutinho, Structure and electronic properties of hydrated mesityl oxide: a sequential quantum mechanics/molecular mechanics approach, Theor. Chem. Acc. 131 (2012) 1214.

[51] S. Canuto, K. Coutinho, From hydrogen bond to bulk: solvation analysis of the n-π^* transition of formaldehyde in water, Int. J. Quant. Chem. 77 (2000) 192–198.
[52] Solvent effects on the UV-visible absorption spectrum of benzophenone in water: a combined Monte Carlo quantum mechanics study including solute polarization, J. Chem. Phys. 126 (2007) 034507.
[53] L.M. Cornetta, K. Coutinho, M.T. d. N. Varella, Solvent effects on the π^* shape resonances of uracil, J. Chem. Phys. 152 (2019) 084301.
[54] A.D. Becke, Density-functional thermochemistry. III. The role of exact exchange, J. Chem. Phys. 98 (1993) 5648–5652.
[55] C. Lee, W. Yang, R.G. Parr, Development of the Colle-Salvetti correlation-energy formula into a functional of the electron density, Phys. Rev. B 37 (1988) 785–789.
[56] R. Improta, V. Barone, G. Scalmani, M.J. Frisch, A state-specific polarizable continuum model time dependent density functional theory method for excited state calculations in solution, J. Chem. Phys. 125 (2006) 054103.
[57] R. Improta, G. Scalmani, M.J. Frisch, V. Barone, Toward effective and reliable fluorescence energies in solution by a new state specific polarizable continuum model time dependent density functional theory approach, J. Chem. Phys. 127 (2007) 074504.
[58] J. Tomasi, B. Mennucci, R. Cammi, Quantum mechanical continuum solvation models, Chem. Rev. 105 (2005) 2999–3094.
[59] C.M. Breneman, K.B. Wiberg, Determining atom-centered monopoles from molecular electrostatic potentials. The need for high sampling density in formamide conformational analysis, J. Comput. Chem. 11 (1990) 361–373.
[60] R.L. Martin, Natural transition orbitals, J. Chem. Phys. 118 (2003) 4775–4777.
[61] M.J. Frisch, G.W. Trucks, H.B. Schlegel, G.E. Scuseria, M.A. Robb, J.R. Cheeseman, G. Scalmani, V. Barone, B. Mennucci, et al., G. A. P. Gaussian09 Revision D.01. 2009, Gaussian Inc. Wallingford CT, 2009.
[62] P. Ahlström, A. Wallqvist, S. Engström, B. Jönsson, A molecular dynamics study of polarizable water, Mol. Phys. 68 (1989) 563–581.
[63] D.N. Bernardo, Y. Ding, K. Krogh-Jespersen, R.M. Levy, An anisotropic polarizable water model: incorporation of all-atom polarizabilities into molecular mechanics force fields, J. Phys. Chem. 98 (1994) 4180–4187.
[64] B.D. Bursulaya, J. Jeon, D.A. Zichi, H.J. Kim, Generalized molecular mechanics including quantum electronic structure variation of polar solvents. II. A molecular dynamics simulation study of water, J. Chem. Phys. 108 (1998) 3286–3295.
[65] L.D. Site, A. Alavi, R.M.L. Bell, The electrostatic properties of water molecules in condensed phases: an ab initio study, Mol. Phys. 96 (1999) 1683–1693.
[66] P.L. Silvestrelli, M. Parrinello, Water molecule dipole in the gas and in the liquid phase, Phys. Rev. Lett. 82 (1999) 3308–3311.
[67] B. Chen, J.J. Potoff, J.I. Siepmann, Adiabatic nuclear and electronic sampling Monte Carlo simulations in the Gibbs ensemble: application to polarizable force fields for water, J. Phys. Chem. B 104 (2000) 2378–2390.
[68] W.R. Rocha, K. Coutinho, W.B. de Almeida, S. Canuto, An efficient quantum mechanical/molecular mechanics Monte Carlo simulation of liquid water, Chem. Phys. Lett. 335 (2001) 127–133.
[69] K. Coutinho, R. Guedes, B. Costa Cabral, S. Canuto, Electronic polarization of liquid water: converged Monte Carlo-quantum mechanics results for the multipole moments, Chem. Phys. Lett. 369 (2003) 345–353.
[70] M. Sharma, R. Resta, R. Car, Dipolar correlations and the dielectric permittivity of water, Phys. Rev. Lett. 98 (2007) 247401.
[71] J.A. Morrone, R. Car, Nuclear quantum effects in water, Phys. Rev. Lett. 101 (2008) 017801.
[72] H.C. Georg, S. Canuto, Electronic properties of water in liquid environment. A sequential QM/MM study using the free energy gradient method, J. Phys. Chem. B 116 (2012) 11247–11254.
[73] L. Shi, Y. Ni, S.E.P. Drews, J.L. Skinner, Dielectric constant and low-frequency infrared spectra for liquid water and ice Ih within the E3B model, J. Chem. Phys. 141 (2014) 084508.
[74] C. Bistafa, Y. Kitamura, M.T.C. Martins-Costa, M. Nagaoka, M.F. Ruiz-López, Cost-effective method for free-energy minimization in complex systems with elaborated ab initio potentials, J. Chem. Theory Comput. 14 (2018) 3262–3271, PMID: 29741887.
[75] I. Bakó, J. Daru, S. Pothoczki, L. Pusztai, K. Hermansson, Effects of H-bond asymmetry on the electronic properties of liquid water – an AIMD analysis, J. Mol. Liq. 293 (2019) 111579.
[76] B. Han, C.M. Isborn, L. Shi, Determining partial atomic charges for liquid water: assessing electronic structure and charge models, J. Chem. Theory Comput. 17 (2021) 889–901.
[77] Y.S. Badyal, M.-L. Saboungi, D.L. Price, S.D. Shastri, D.R. Haeffner, A.K. Soper, Electron distribution in water, J. Chem. Phys. 112 (2000) 9206–9208.
[78] S.A. Clough, Y. Beers, G.P. Klein, L.S. Rothman, Dipole moment of water from Stark measurements of H2O, HDO, and D2O, J. Chem. Phys. 59 (1973) 2254–2259.